JOURNAL OF AIRCRAFT
Vol. 31, No. 2, March–April 1994

Analysis of Aerodynamics of Airfoils Moving over a Wavy Wall

Kyoko Nitta*
Nagoya University, Aichi 464-01, Japan

The aerodynamic characteristics and the motion of a two-dimensional flat plate airfoil flying over a wavy wall surface are calculated. The used computational scheme is a finite difference method (ADI scheme), which was developed to improve the Ames code LTRAN2 and to expand the computable reduced frequency region up to 0.8. Modifications of the grid generating system is the major point for applying the LTRAN2 version to the current problem. Weak compressibility (M_∞ = 0.1–0.3) is considered, but nonlinearity is neglected in current calculations. Numerical computations include cases of a flat plate flying over a flat solid wall in addition to the cases of a moving wavy wall. The flat plate is fixed in the freestream at first, and after some research of its aerodynamic characteristics, aeroelastic analysis is added allowing 3 DOFs. The calculated results are compared with those obtained by the lifting surface theory. The agreement is satisfactory.

Nomenclature

a = pitch axis location, referenced to midchord, in semichord
b = semichord length
C_L, C_M, C_N = coefficients of lift, moment about pitching axis, and control surface moment about hinge axis, respectively
C_p = pressure coefficient
c = hinge axis location, referenced to midchord, in semichord
H = distance between airfoil and wall surface nondimensionalized by b
h, h_a = plunging DOF and h/b
h_w = amplitude of wavy wall surface nondimensionalized by b
I_α = polar moment of inertia of airfoil mass about elastic axis
I_β = polar moment of inertia of control surface mass about hinge axis
k = reduced frequency of oscillation based on semichord
k_h, k_α, k_β = $\omega_h b/U_\infty$, $\omega_\alpha b/U_\infty$, and $\omega_\beta b/U_\infty$, respectively
k_w = reduced frequency of wavy wall surface based on semichord
l = wave length of wavy wall surface nondimensionalized by b
M_∞, U_∞ = freestream Mach number and velocity, respectively
m = mass of the airfoil per unit span
r_α, r_β = $\sqrt{I_\alpha/mb^2}$ and $\sqrt{I_\beta/mb^2}$, respectively
S_α = airfoil static moment about elastic axis
S_β = control surface static moment about hinge axis
t = time
w_w = downwash on wavy wall surface
x, y = orthogonal coordinates nondimensionalized by b
x_α, x_β = S_α/mb and S_β/mb, respectively
α = angle of incidence, or pitching DOF
β = control surface pitching DOF
γ = specific heat ratio
Δx, Δy = grid spacing in x and y directions, respectively
η_m = absolute value of computational coordinate of wall surface
μ = airfoil-air mass ratio, $m/\pi\rho b^2$
ν = velocity ratio
ξ, η = orthogonal coordinates in computational domain
ϕ = perturbation velocity potential
ω_h, ω_α, ω_β = uncoupled natural frequencies of plunging, pitching about elastic axis, and control surface pitching about hinge axis, respectively

Introduction

IN the takeoff and landing phases, airplanes must fly in ground effects. Some of them must fly in ground effects all through the cruising, such as ram wings which fly just over the water surface. Recently, because of increasing demand of commuter transportation, the topics on air cushion vehicles (ACV) seem to be discussed vigorously again. In this article the wavy wall problem is considered using a finite difference method.

A lot of reports were presented on the ordinary ground effect problem, namely the cases of the flat surface ground. Most of them adopted a numerical approach such as the vortex lattice method, while others present analytical solutions, e.g., using conformal mapping.[1] A practical view of this problem is shown in the comprehensive study carried out by Pistolesi.[2] There also have been numerous researches for cases of steady[3] and unsteady,[4] or two-dimensional[5] and three-dimensional and unsteady[6] problems. In the view of application, there are options like the aerodynamics of racing cars,[7] gust response of three-dimensional wing,[8] and stability analysis.[9] Many of them use the concept of a mirror image wing, which was first developed by Wieselsberger.[10] Experimental approaches are available.[11]

For the wavy wall surface, however, there are very few published reports. There exists the exact aerodynamic solution, even when the shape of the wall surface is wavy if the wall is fixed in the domain, i.e., cases of the steady problem.[12] For the cases of unsteady problem (i.e., when the wavy wall moves), Ballows and Widnall[13] carried out interesting analyses by using the method of matched asymptotic expansions of Van Dyke. They investigated the aerodynamics and 2-DOF (pitch and plunge) motion of the wing. Their study included the cases of two- and three-dimensional wings with thickness. Ando and Ichikawa[14] recently solved the aerodynamic characteristics of a thin airfoil flying in proximity to a moving

Received May 4, 1992; revision received Jan. 26, 1993; accepted for publication March 10, 1993. Copyright © 1993 by the American Institute of Aeronautics and Astronautics, Inc. All rights reserved.

*Research Associate, Department of Aeronautical Engineering, Furo-cho, Chikusa-ku, Nagoya-shi. Member AIAA.

wavy wall surface by using the lifting-surface theory. Ando et al.[15] investigated the motion induced by the wavy wall by using the lifting-surface method.

In Refs. 13–15, the most fundamental typical cases are considered, where a two-dimensional flat plate flies in the direction normal to the wave-crest-line. The wave moves keeping the harmonic motion with its surface solid. The fluid is assumed incompressible, and all the disturbances are sufficiently small to permit linearized treatments.

A finite difference method (FDM) is adopted this time to calculate the aerodynamic characteristics based on the same assumption discussed previously. The results obtained are compared with those obtained by the lifting-surface method (LSM) in Ref. 14. In Ref. 14, calculated results are compared with those in Ref. 7, therefore, we can examine the reliability of our computer code in comparison with LSM in Ref. 14. For the FDM computational scheme, the method of Ref. 16, a version of LTRAN2,[17] is used with some modifications to introduce the wall surface under the airfoil. This version of LTRAN2 includes the higher order term with respect to time in the governing differential equation and boundary conditions, and permit the maximum computable reduced frequency up to 0.8. In adoption, however, some simplifications are introduced at the same time for restricting us within a low Mach number region ($M_\infty \leq 0.3$). The nonlinear treatment in the Ref. 16 version of LTRAN2 is also dropped and only the flat plate airfoil is treated. It is necessary for comparison with the results of LSM. Currently, the LSM code can only compute incompressible cases. No aircraft flies very fast in proximity to the ground, therefore, it would be an acceptable assumption.

Aeroelastic motions induced by the aerodynamic forces are presented next in this article. There are classic good textbooks such as Bisplinghoff et al.[18] to illustrate the dynamic response problem. Using LTRAN2 and/or its versions, there are many reports treating the aeroelastic problem in a similar manner. Time response analysis is available with this kind of approach, and was first carried out by Ballhaus and Goorjian.[19] In these works, structural and aerodynamic equations are solved simultaneously. There are variations in details, e.g., in dealing with the aerodynamic integration. In this article, the aerodynamic forces are calculated using FDM including the moving wavy wall. As the wavy wall moves continuously, the problem becomes a forced oscillation as a result of the aerodynamic forces induced by the bumps of the moving wavy wall. After the transient motion dies, the harmonic solution is left. So again we can compare the results with LSM presented in Ref. 15. Because there seems to be no other comparable results which can be used throughout this article, we restrict our comparison only with LSM.

Formulation

Governing Differential Equation

The computational scheme is taken from Ref. 16 which is a version of the transonic code LTRAN2. We call it simply "the version" in this article. The governing differential equation is based on the unsteady small perturbation equation for the two-dimensional ϕ, which is the same as the version. The second time-differential term $M_\infty^2\phi_{tt}$ is included in the version. The version also includes the nonlinear term $[-(\gamma + 1)M_\infty^m\phi_x/2]_x$, but for linearization to compare the results with LSM, γ is set to -1 all through the current calculations. We use the Cartesian coordinates x, y (nondimensionalized by b) and t (nondimensionalized by b/U_∞)

$$M_\infty^2\phi_{tt} + 2M_\infty^2\phi_{xt} = (1 - M_\infty^2)\phi_{xx} + \phi_{yy} \qquad (1)$$

for our calculation. The version uses the chord length for nondimensionalization. But for comparison with LSM which is based on b, and also for convenience in the subsequent aeroelastic analysis, we use b for the characteristic length for normalization.

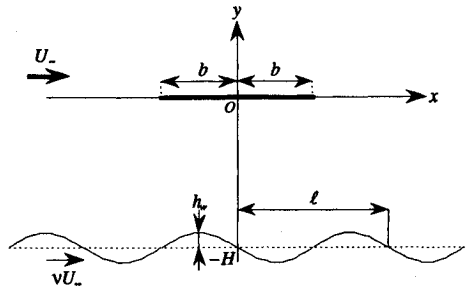

Fig. 1 Wavy wall problem.

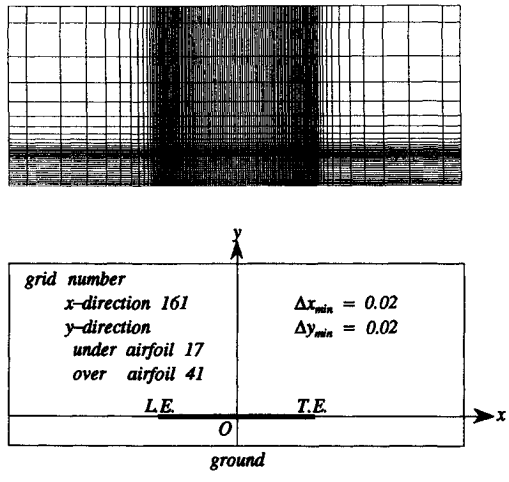

Fig. 2 Mesh pattern near airfoil for aerodynamic calculations for $H = 0.4$.

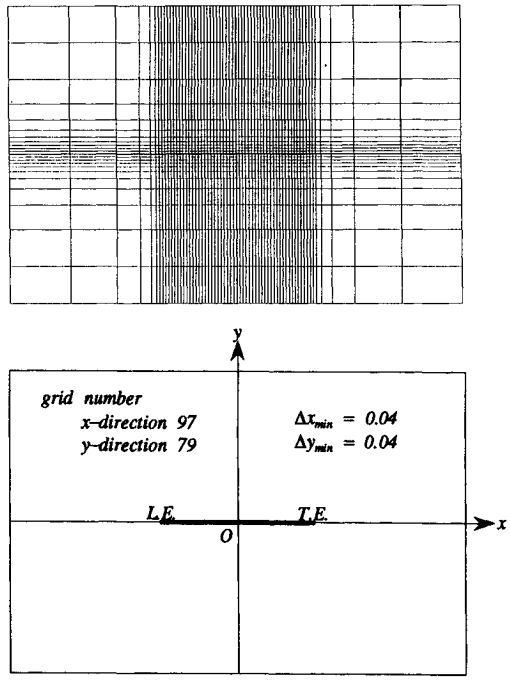

Fig. 3 Original mesh near airfoil.

Wavy Wall Surface

A flat plate airfoil is located in the freestream U_∞ in x direction. Under the airfoil, an infinite wavy wall surface travels with the travel velocity νU_∞ whose mean line lies on $y = -H$, and the wave amplitude is h_w (Fig. 1). For simplicity, the wall surface is assumed to keep harmonic motion. The vertical displacement of the wall surface is then expressed as follows:

$$y = -H + h_w \sin[k_w(t - x/\nu)] \qquad (2)$$

where we assume $h_w << H$ (small disturbance). All the values except t are nondimensionalized by b. k_w is defined as $k_w \equiv 2\pi\nu/l$.

The ordinary tangency boundary condition is satisfied on the surface of the airfoil and on the wall surface. Boundary conditions are formulated very easily following the same method as on the airfoil's upper surface. The normal wash on the wall surface w_w is given by

$$w_w = h_w k_w(1 - 1/\nu)\cos[k_w(t - x/\nu)] \tag{3}$$

It is noteworthy that the airfoil cannot be aware of the wavy wall surface, if $\nu = 1$. As can be seen in Eq. (3), disturbances of the stream due to the wavy wall surface itself diminish when the wavy wall moves with the same velocity as the freestream.

Grid Generation

In order to introduce the wall surface into the considered region, the grid generation system must be revised. The original grid system of the version uses polynomials to stretch the grid. We adopt the same concept as the original system to create the grid system suitable for our problem. The guidelines of the grid generation system are presented below. The physical coordinates are represented by x, y, and the computational ones are by ξ, η.

1) Whole grid shapes are square in the computational domain, which covers $-2 \le \xi \le 2$ and $-\eta_m \le \eta \le 1$. Here, $-\eta_m$ represents the vertical computational coordinate for the wall surface ($0 < \eta_m < 1$). In case of the wavy wall problem, it means the mean wall line. Note that the airfoil is located at $-1 \le \xi \le 1$ and $\eta = 0$ in the computational domain.

2) In x direction and in positive y direction, the grids are constructed using the same stretching functions as the version.

3) In negative y direction, i.e., below the airfoil, the grid generating polynomial must be rewritten. The grid spacing should be closer near the airfoil and the wall. The mapping relation of y vs η between the airfoil and the wall is determined after the manner of x vs ξ between both edges of the airfoil.

4) It would be desirable to make the minimum mesh shapes square in the physical domain, i.e., $\Delta x = \Delta y$ near both edges of the airfoil and on the wall just below the edges. Here, Δx and Δy mean the physical grid spacing in x and y directions.

Figure 2 shows an example of the grid pattern obtained following the above mentioned guidelines. Figure 3 shows the version's grid pattern for comparison. The minimum mesh size in Fig. 2 is set to a quarter of the version's size because the length of interest in the current problem is the height instead of the chord length. Unless otherwise mentioned, the height of the airfoil H is set to 0.4, about a quarter of the chord length. The grid pattern in Fig. 2 is used in the aerodynamic calculations presented afterwards. All the calculations are performed in $-200 \le x \le 200$ and $-H \le y \le 200$ in the physical domain.

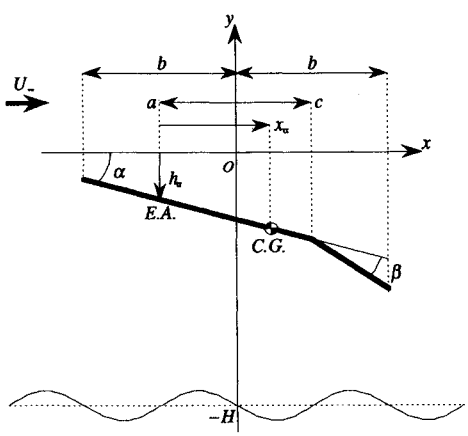

Fig. 4 Definition of parameters for 3-DOF aeroelastic analysis.

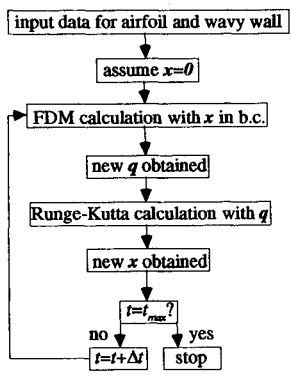

Fig. 5 Flow chart of calculating motion over wavy wall.

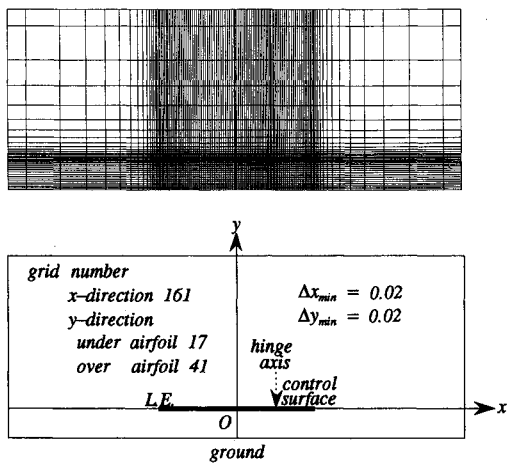

Fig. 6 Mesh pattern modified to introduce control surface; $c = 0.5$, $H = 0.4$.

Aeroelastic Analysis (3-DOF Wing)

Equations of Motion and Solution Technique

The problem treated here is the oscillation of the airfoil as a result of the aerodynamic perturbation induced by the wavy wall. The flat plate airfoil moves with 3 DOFs [i.e., pitch (α), plunge (h), and control surface pitch (β)]. Its motion is governed by[18]

$$\begin{aligned} m\ddot{h} + S_\alpha\ddot{\alpha} + S_\beta\ddot{\beta} + m\omega_h^2 h &= -L \\ S_\alpha\ddot{h} + I_\alpha\ddot{\alpha} + [(c - a)bS_\beta + I_\beta]\ddot{\beta} + I_\alpha\omega_\alpha^2\alpha &= M \\ S_\beta\ddot{h} + [(c - a)bS_\beta + I_\beta]\ddot{\alpha} + I_\beta\ddot{\beta} + I_\beta\omega_\beta^2\beta &= N \end{aligned} \tag{4}$$

where the dots denote differentiation with respect to physical time.

When normalized by b and through some mathematical manipulation, we get

$$x' = Ax + Bq \tag{5}$$

where

$$x^T = (h_a\ \alpha\ \beta\ h_a'\ \alpha'\ \beta')^T, \qquad q^T = (-C_L\ C_M\ C_N)^T$$

$$A = \begin{bmatrix} 0 & \mathrm{I} \\ M^{-1}K & 0 \end{bmatrix}, \qquad B = \frac{1}{\pi\mu}\begin{bmatrix} 0 \\ M^{-1} \end{bmatrix}$$

$$M = \begin{bmatrix} 1 & x_\alpha & x_\beta \\ x_\alpha & r_\alpha^2 & (c - a)x_\beta + r_\beta^2 \\ x_\beta & (c - a)x_\beta + r_\beta^2 & r_\beta^2 \end{bmatrix}$$

$$K = \begin{bmatrix} -k_h^2 & 0 & 0 \\ 0 & -r_\alpha^2 k_\alpha^2 & 0 \\ 0 & 0 & -r_\beta^2 k_\beta^2 \end{bmatrix}$$

For nondimensionalization, the vertical displacement (positive downwards) h is replaced by $h_a \equiv h/b$, and uncoupled circular frequencies ω_i ($i = h, \alpha, \beta$) are replaced by reduced frequencies $k_i \equiv \omega_i b/U_\infty$. The prime represents differentiation with respect to nondimensional time. Other symbols are shown in Fig. 4. Equation (5) is a set of differential equations to be solved step-by-step following the change of the flowfield, which is calculated with FDM using h_a, α, β, and their derivatives obtained in the previous time step for the boundary condition of the airfoil. A standard Runge-Kutta method is used for the structural integration to solve Eq. (5) at each step immediately after the aerodynamic coefficients C_L (lift), C_M (moment of the airfoil around the elastic axis), and C_N (moment of the control surface around the hinge axis) are obtained. The time step sizes used in aerodynamic and structural response calculations are the same. The flow chart of the above procedure is shown in Fig. 5.

Mesh Refinement for the Addition of Control Surface

In this calculation, it would be better to rewrite the mesh generation guidelines. As the control surface is added to the system, the grid spacing whose concept is the same as the one used on the original airfoil is introduced to the two parts of the airfoil: forward and aft of the hinge axis position. The new guidelines are as follows:

1) All grid shapes are square in the computational domain.

2) In positive y direction, the grids are constructed using the same stretching functions as the version. In negative y direction, the grids are generated in the same way described before.

3) In x direction, the grids are newly constructed. The grid spacing is smaller near the leading and trailing edges and also near the hinge axis. The mapping relation of x vs ξ between the leading edge and the hinge axis, the hinge axis and the trailing edge are determined after the manner of x vs ξ between both edges of the airfoil of the original mesh pattern.

4) It would be desirable to make the minimum mesh shapes square in the physical domain, i.e., $\Delta x = \Delta y$ near both edges of the airfoil and the hinge axis, and on the wall below them.

The example mesh pattern is seen in Fig. 6. The division number on the airfoil and minimum mesh size remain the same as before. This mesh pattern is used in the calculation of 3-DOF wing motion. The hinge axis is located at $x = 0.5$ all through the calculations.

Results and Discussion

Aerodynamic Characteristics (Wing Fixed)

In order to check the current computer code, numerical computations are started with cases with the flat wall surface

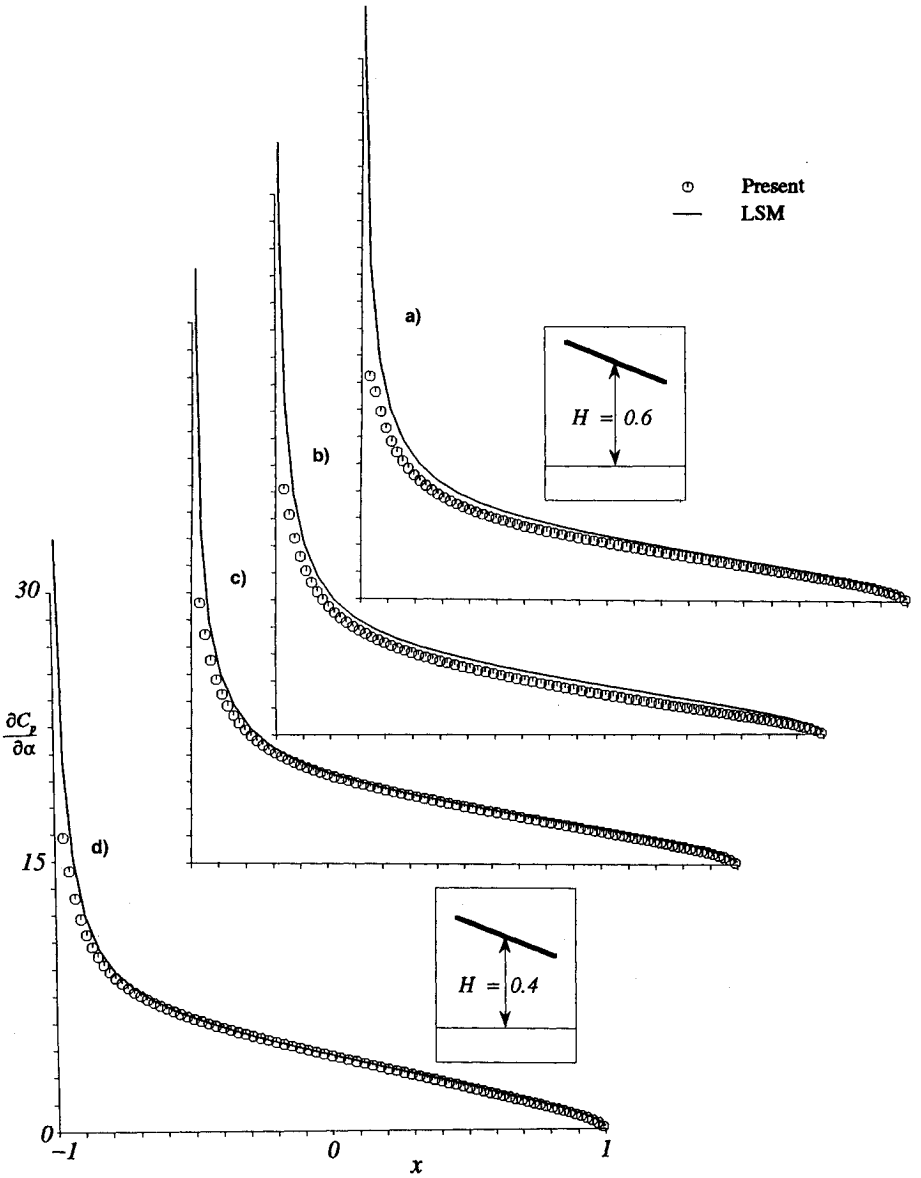

Fig. 7 Chordwise pressure distribution ($\partial C_p/\partial\alpha$) over flat wall surface with incidence: a) $H = 0.6$, $M_\infty = 0.1$; b) $H = 0.6$, $M_\infty = 0.2$; c) $H = 0.6$, $M_\infty = 0.3$; and d) $H = 0.4$, $M_\infty = 0.3$.

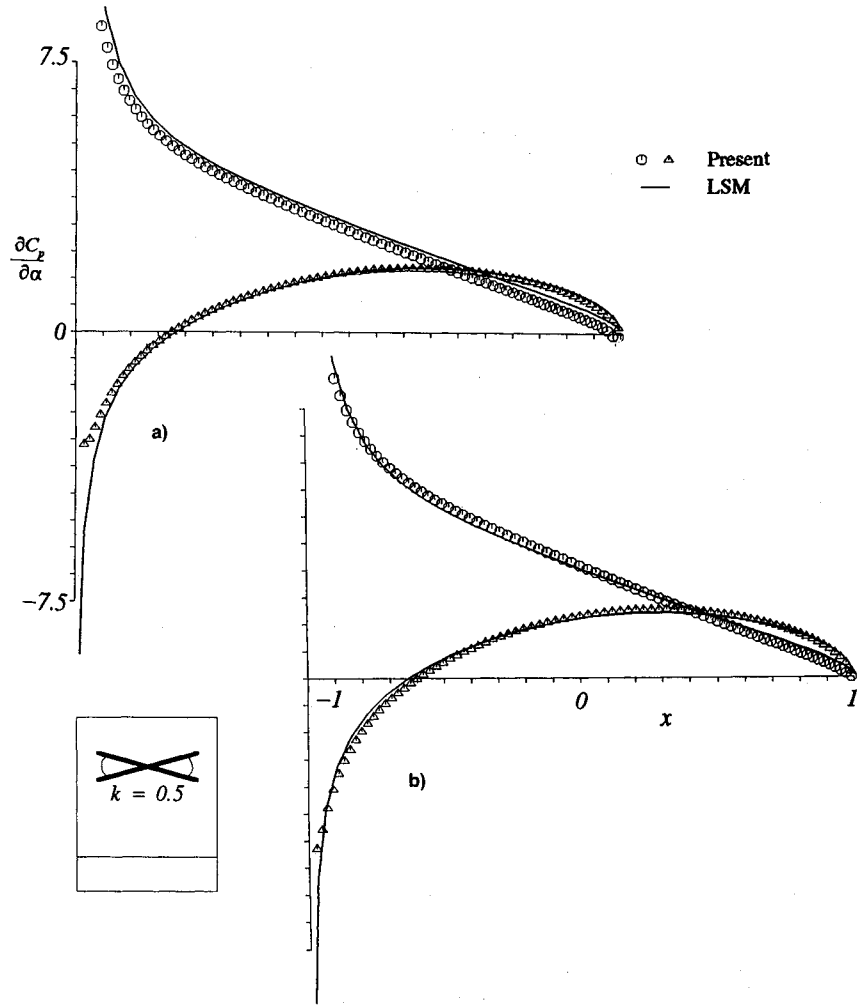

Fig. 8 Chordwise pressure distribution ($\partial C_p/\partial\alpha$) over flat wall surface for pitching around midchord with $k = 0.5$: a) $M_\infty = 0.1$ and b) $M_\infty = 0.3$.

whose results can be obtained from LSM using the mirror-image wing. Because the original computer code LTLAN2 is for transonic, the results for $M_\infty < 0.1$ are rather poor. Therefore, most of computations are made using $M_\infty = 0.3$, which may be nominally regarded as "incompressible case." Figure 7 shows the pressure distribution for the steady case. The unsteady case is treated in Fig. 8 where the airfoil is oscillated around midchord with the reduced frequency, $k = 0.5$. The solid curves are LSM results of $M_\infty = 0$. The FDM results for $M_\infty = 0.3$ agree better with those of LSM than for M_∞ in the range 0.1 to 0.2.

Next, the problem with the moving wavy wall is considered. Figure 9 shows the pressure distribution for different parameters for the wavy wall. The case for Figs. 9a and 9b is the particular case where the result for $M_\infty = 0.1$ agrees better with the LSM result than one for $M_\infty = 0.3$. It may due to the high frequency of the wall. All the other calculations are made with $M_\infty = 0.3$. The agreement between both methods is satisfactory. Aerodynamic loading decreases when ν approaches unity as discussed before.

For the sake of comparison of the results between FDM and LSM, zero incidence cases only are treated in Fig. 9. However, it is of course an unnecessary restriction for the current approach. Since the linear theory is employed, C_L can be written as a function of α and h_w by

$$C_L(\alpha, h_w) = C_L|_{\alpha=h_w=0} + \frac{\partial C_L}{\partial \alpha}\cdot\alpha|_{h_w=0} + \frac{\partial C_L}{\partial h_w}\cdot h_w|_{\alpha=0}$$

$$+ O(\alpha^2, h_w^2, \alpha h_w) \cong \frac{\partial C_L}{\partial \alpha}\cdot\alpha|_{h_w=0} + \frac{\partial C_L}{\partial h_w}\cdot h_w|_{\alpha=0} \qquad (6)$$

Figure 10 compares the lift of the cases with (Fig. 10a) and without (Fig. 10b) α over the moving wavy wall whose amplitude is one-tenth of the wing height. Figure 10a stands for the right side of Eq. (6). The distance between the two curves represents the first term in the right side of Eq. (6), which is the lift for the case of Fig. 7d, while the second term is represented by the curve Fig. 10b, which is the lift for the case of Fig. 9d. The concept above will be valid for cases where α are replaced by any airfoil camber.

Convergence and Computational Time

Figure 11 shows an example of the convergence property of FDM.

Figures 11a and 11b correspond to Fig. 7d and Fig. 9c, respectively. The lowest sinusoidal curve shows the wall-surface height just under the midchord of the airfoil. The data in Fig. 11b are obtained using 360 time steps per cycle and the marks on the curve show the values at each 36 time step increment. The lift coefficient becomes harmonic after 3 cycles. Compared with Fig. 10, it takes more time to converge because of higher frequency. The total computational time up to five cycles is about one and a half minutes, using FACOM M-1800.

Results of the Aeroelastic Analysis

The flow disturbance induced by the harmonic wavy wall leads the airfoil motion to become harmonic after the initial transient solution of the differential equation diminishes; so we can compare the results with the ones from LSM again. The LSM technique used in Ref. 15 is adopted.

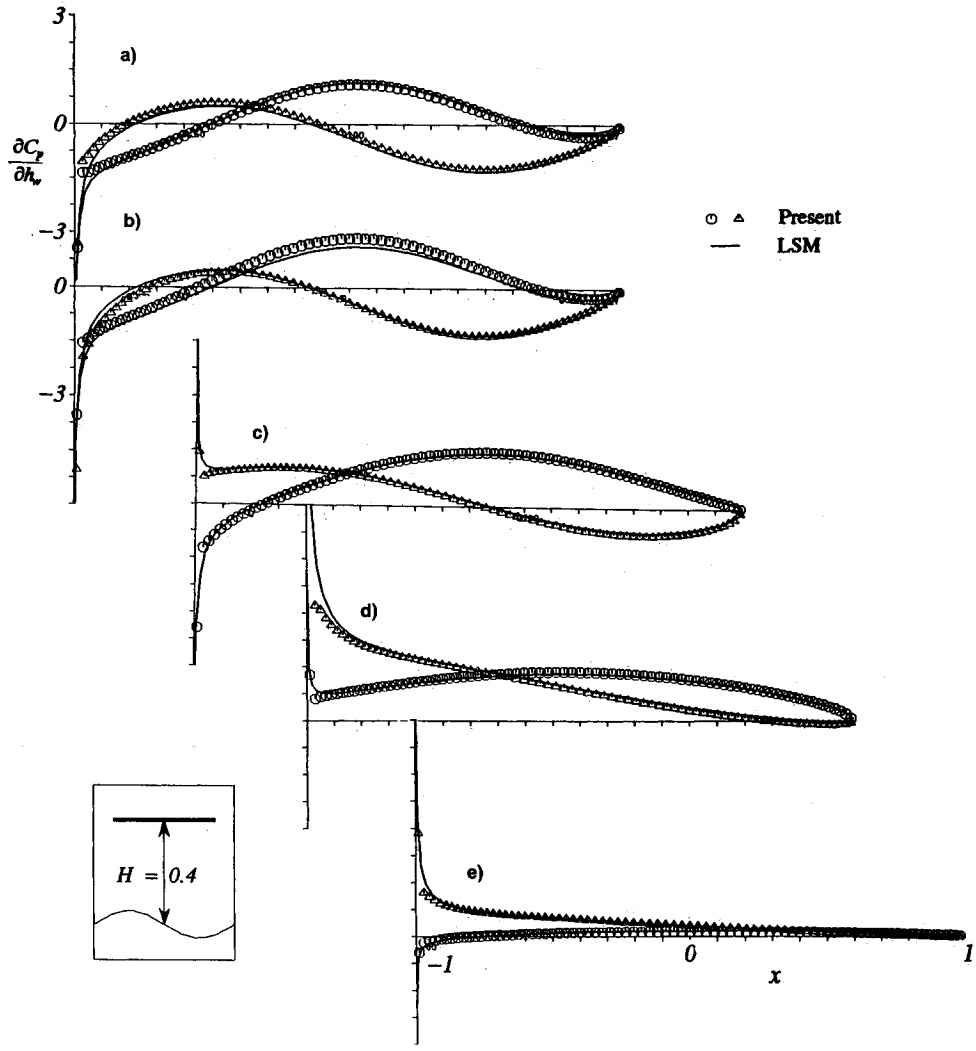

Fig. 9 Chordwise pressure distribution ($\partial C_p/\partial h_w$) over wavy wall surface: a) $l = 2.0$, $\nu = 0.3$, $k_w = 0.9425$, $M_\infty = 0.1$; b) $l = 2.0$, $\nu = 0.3$, $k_w = 0.9425$, $M_\infty = 0.3$; c) $l = 3.0$, $\nu = 0.3$, $k_w = 0.6283$; d) $l = 5.0$, $\nu = 0.3$, $k_w = 0.3770$; and e) $l = 5.0$, $\nu = 0.7$, $k_w = 0.8796$.

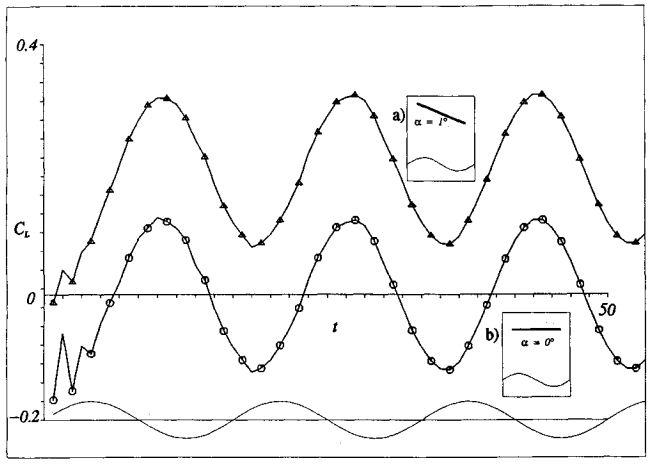

Fig. 10 Aerodynamic loading comparison between airfoils with and without incidence over wavy wall surface of $k_w = 0.3770$: a) $\alpha = 1$ deg and b) $\alpha = 0$ deg.

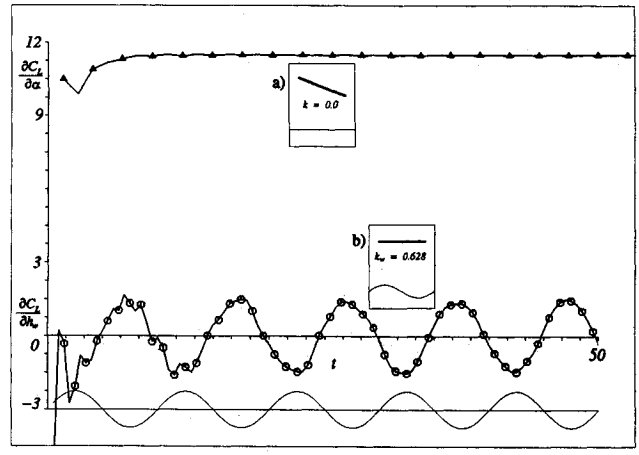

Fig. 11 Convergence property: a) steady case (over flat wall surface with incidence) and b) unsteady case (over wavy wall surface of $k_w = 0.6283$ without incidence).

In Ref. 15 only 2-DOF systems are treated. For the sake of comparison, a similar technique is used to obtain the results from LSM including the control surface. Because it is not the purpose of this article to explain the LSM technique, details are not shown here (see Appendix). 2-DOF systems were also dealt with in the first stage of the aeroelastic research, and the results were identical to FDM and LSM methods.

Introducing the control surface into the domain, before calculating the motion induced by the wavy wall, the check of mesh property was done with the case of forced vibration of the control surface over the flat surface. The pressure distribution is shown in Fig. 12. Figure 12a is with the mesh of Fig. 2, and Fig. 12b is with the modified one of Fig. 6. The solid curve is obtained using LSM mirror image code. The

agreement is satisfactory with both meshes, however, it can be seen that in Fig. 12b, the agreement near the hinge axis is significantly improved compared with Fig. 12a.

Here in 3-DOF systems, parameters commonly used for the presented results are listed below:

$$k_h/k_w = 6.0, \quad k_\alpha/k_w = 8.0, \quad k_\beta/k_w = 10.0$$

$$r_\alpha^2 = 0.25, \quad x_\beta = 0.0, \quad a = -0.5$$

$$H = 0.4, \quad h_w = 0.04, \quad \nu = 0.3$$

The amplitude of each parameter after the convergence to the harmonic motion also agrees with the one obtained with LSM. Some of them are shown in Table 1. In both cases in Table 1, $r_\beta^2 = 0.05$.

Table 1 Comparison of amplitudes of variables using FDM and LSM after convergence to harmonic motion

	a) $\mu = 10$, $l = 5$, $x_a = 0.0$		b) $\mu = 20$, $l = 8$, $x_a = 0.2$	
	Present	LSM	Present	LSM
C_L	0.12	0.1223	0.13	0.1308
$\lvert h_a \rvert \times 10^3$	0.77	0.7757	0.10	0.1059
$\lvert \alpha \rvert \times 10^3$	0.51	0.5039	0.47	0.4071
$\lvert \beta \rvert \times 10^3$	0.12	0.1217	0.12	0.1250

The time histories of C_L, C_M, C_N, h_a, α, and β for Table 1a are in Fig. 13. The scaling of the vertical axes depends on the maximum values of each variable, not on the amplitudes.

The convergence of β is the worst of all, and the maximum value of the transient part is bigger compared with the others. There are some reasons to explain this.

One of them is that we set the airfoil in the free motion from the beginning of the calculations. The typical analyses with LTRAN2 or its versions set the airfoil in the forced vibration at first, and after the aerodynamic forces become harmonic, its free motion starts.[19] In the current calculations, we did not follow this procedure. So we have to think of the transient part as the mixture of aerodynamic and aeroelastic responses, and also numerical instability of computation.

The poor convergence also comes from the large value of r_β. In Fig. 13, $r_\beta^2 = 0.05$. Cases with smaller r_β show good convergence behavior. If we use $r_\beta^2 = 0.0064$, the time histories become Fig. 14. However, numerical experiments performed afterwards indicate that the effects of the other DOF, plunging and pitching, often strongly affects the motion of the control surface.

For the comparison with LSM, some comments are given here. The results of FDM strongly depend on the procedure of discretization. On the other hand, LSM results are not so sensitive to the computational condition, such as the number of the control points. Moreover, the aerodynamic results of LSM[14] are checked with previous reports,[7] therefore we can regard them as "exact solutions." However, it must be men-

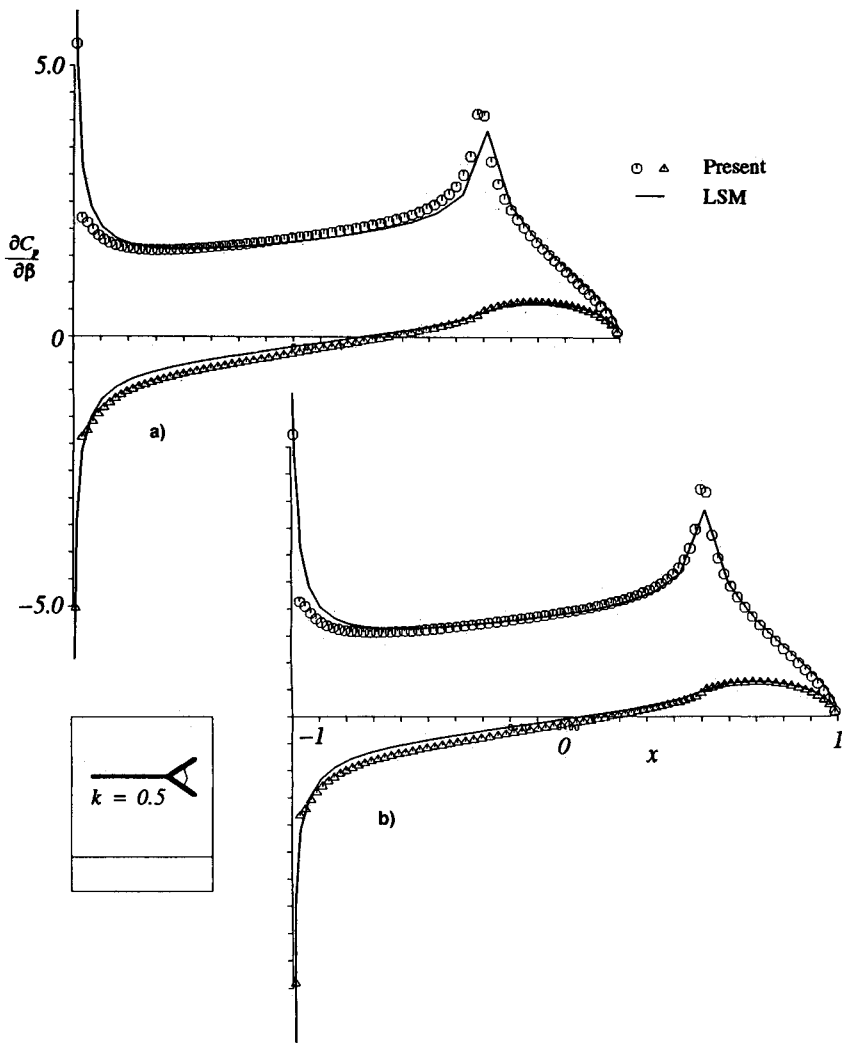

Fig. 12 Chordwise pressure distribution ($\partial C_p/\partial\beta$) over flat wall surface for control surface pitching with $k = 0.5$: a) mesh of Fig. 2 used and b) mesh of Fig. 6 used.

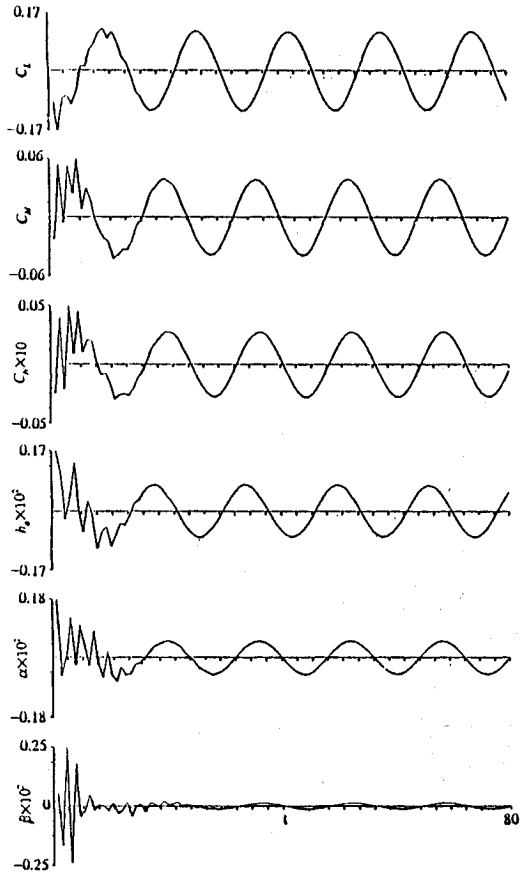

Fig. 13 Time history of variables of 3-DOF airfoil over wavy wall surface; $k_w = 0.3770$, $r_\beta^2 = 0.05$.

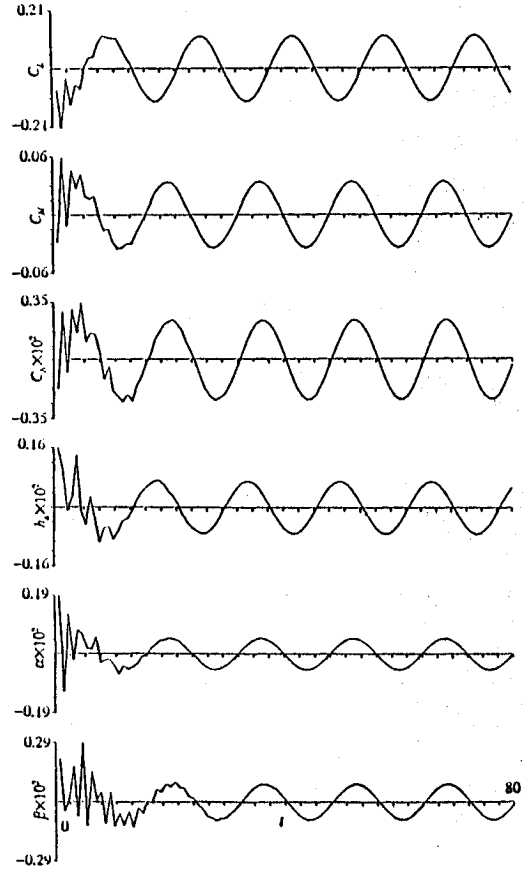

Fig. 14 Time history of variables of 3-DOF airfoil over wavy wall surface; $k_w = 0.3770$, $r_\beta^2 = 0.0064$.

tioned that the results of LSM with the wing motion[15] are valid only on the assumption that the reduced frequency of the wavy wall is very far from the uncoupled natural frequencies of the airfoil, such as the cases treated here. In the calculation of LSM, all the variables are assumed to keep harmonic motion with k_w (see Appendix). In the actual situation, however, there must be some coupling of modes of the airfoil's DOFs and/or aerodynamic modes induced by the wave motion. The effect of coupling may be negligible only if the natural frequencies are far from each other and from the frequency of the wavy wall. In other words, in cases of allowing DOFs, we can use the results from LSM only as "approximated solutions." The results of FDM are considered to be nearer to the exact solutions in such cases.

Conclusions

The aerodynamics and 3-DOF motion of a flat plate airfoil flying over a moving wavy wall surface were computed using a finite difference method. The method was derived from a version of LTRAN2 while introducing the wall surface. The mesh generation systems were modified according to the cases considered. The results were compared with the ones based on the lifting surface theory and the agreement was quite satisfactory.

Appendix

A quick view of LSM approach of analysis of motion is given. The technique adopted here follows the one presented in Ref. 15.

The normal wash on the 3-DOF flat plate, w_a is given by

$$w_a = -h_a' - \alpha - \alpha'(x_s - a) - 1(x_s, c)[\beta + \beta'(x_s - c)]$$

$$1(x_s, c) \equiv \begin{cases} 0 & -1 \le x_s < c \\ 1 & c \le x_s \le 1 \end{cases} \tag{A1}$$

where all values except w_a are nondimensionalized by b and w_a, by U_∞, x_s is the x coordinate of the control point. If we use Eq. (4) and rewrite the aerodynamic coefficients

$$C_L = \int_{-1}^{1} C_{ps}\, dx_s$$

$$C_M = \int_{-1}^{1} C_{ps}(x_s - a)\, dx_s \tag{A2}$$

$$C_N = \int_{c}^{1} C_{ps}(x_s - c)\, dx_s$$

and assume the harmonic oscillation with k_w, we can express h_a, α, β as functions of C_{ps}, which is the pressure coefficient on the airfoil surface. Substituting in Eq. (A1), w_a can be expressed as a function of C_{ps}. Then we can get the relationship between w_a and C_{ps}

$$\tilde{w}_a(x) = \int_{-1}^{1} \tilde{C}_{ps}(x_s) G(x, x_s)\, dx_s \tag{A3}$$

where $\tilde{w}_a$ and $\tilde{C}_{ps}$ are complex amplitudes for w_a and C_{ps}, respectively. Then the integral equations described in Ref. 14 are modified including the coefficient G, obtained above. All the other procedures remain the same as described in Ref. 14. For details, see the original papers.

Acknowledgments

The author acknowledges Shigenori Ando, of Tokushima Bunri University, for working with the first part of this research. This research owes him a lot. Thanks are also due to

Masami Ichikawa, Nagoya Agency of Industrial Science and Technology, and Tomonori Kawamoto in our laboratory for their invaluable support.

References

[1]Tomotika, S., Nagamiya, T., and Takenouti, Y., "The Lift on a Flat Plate Placed near a Plane Wall, with Special Reference to the Effect of the Ground upon the Lift of a Monoplane Aerofoil," Rept. of the Aeronautical Research Inst., Tokyo Imperial Univ., Vol. 8, No. 97, 1933.

[2]Pistolesi, E., "Ground Effect—Theory and Practice," NACA TM-828, 1937.

[3]Tuck, E. O., "Hydrodynamic Problems of Ships in Restricted Waters," *Annual Review of Fluid Mechanics*, Vol. 10, 1978, pp. 33, 34.

[4]Chen, Y. S., and Schweikhard, W. G., "Dynamic Ground Effects on a Two-Dimensional Flat Plate," *Journal of Aircraft*, Vol. 22, No. 7, 1985, pp. 638–640.

[5]Bagley, J. A., "The Pressure Distribution on Two-Dimensional Wings Near the Ground," Aeronautical Research Council 3238, London, 1961.

[6]Nuhait, A. O., and Mook, D. T., "Numerical Simulation of Wings in Steady and Unsteady Ground Effects," *Journal of Aircraft*, Vol. 26, No. 12, 1989, pp. 1081–1089.

[7]Katz, J., "Calculation of the Aerodynamic Forces on Automotive Lifting Surfaces," *Transactions of the American Society of Mechanical Engineers*, Vol. 107, Dec. 1985, pp. 438–443.

[8]Kobayakawa, M., and Maeda, H., "Gust Response of a Wing near the Ground Through the Lifting Surface Theory," *Journal of Aircraft*, Vol. 15, No. 8, 1978, pp. 520–525.

[9]Kumar, P. E., "Stability of Ground Effect Wings," College of Aeronautics, Rept. Aero No. 196, Cranfield, May 1967.

[10]Wieselsberger, C., "Wing Resistance near the Ground," NACA TM-77, 1922.

[11]Chawla, M. D., Edwards, L. C., and Franke, M. E., "Wind-Tunnel Investigation of Wing-in-Ground Effects," *Journal of Aircraft*, Vol. 27, No. 4, 1990, pp. 289–293.

[12]Tomotika, S., and Imai, I., "The Interference Effect of the Surface of the Sea on the Lift of a Seaplane," Rept. of the Aeronautical Research Inst., Tokyo Imperial Univ., Vol. 12, No. 146, 1937.

[13]Barrows, T. M., Widnall, S. E., and Richardson, H. H., "The Use of Aerodynamic Lift for Application to High Speed Ground Transportation," Office of High Speed Ground Transportation, FRA-RT-71-56, Washington, DC, June 1970.

[14]Ando, S., and Ichikawa, M., "Aerodynamic Response of a Thin Airfoil Flying over and in Proximity to a Wavy Wall Surface—Lifting Surface Theory," *Transactions of the Japan Society for Aeronautical and Space Sciences*, Vol. 34, May 1991, pp. 1–11.

[15]Ando, S., Sakai, T., and Nitta, K., "Analysis of Motion of Airfoil Flying over Wavy Wall Surface (Lifting Surface Method)," *Transactions of the Japan Society for Aeronautical and Space Sciences*, Vol. 35, May 1992, pp. 27–38.

[16]Nakamichi, J., "An Improved Version of the LTRAN2 for High Frequency Domain," *Transactions of the Japan Society for Aeronautical and Space Sciences*, Vol. 27, Nov. 1984, pp. 121–133.

[17]Ballhaus, W. P., and Goorjian, P. M., "Implicit Finite-Difference Computations of Unsteady Transonic Flows About Airfoils," *AIAA Journal*, Vol. 15, No. 12, 1977, pp. 1728–1735.

[18]Bisplinghoff, R. L., Ashley, H., and Halfman, R. L., "Aeroelasticity," Addison Wesley, Reading, MA, 1955.

[19]Ballhaus, W. P., and Goorjian, P. M., "Computation of Unsteady Transonic Flows by the Indicial Method," *AIAA Journal*, Vol. 16, No. 2, 1978, pp. 117–124.